# Cracking Controls ATP Hydrolysis in the catalytic domain of a P-ATPase

M. Agueda Placenti[ab], Santiago A. Martinez-Gache[ab], Rodolfo M. González-Lebrero[ab], Peter G. Wolynes[c], F. Luis González Flecha[ab*], Ernesto A. Roman[de*].

[a]Universidad de Buenos Aires, Facultad de Farmacia y Bioquímica, Junín 954 -C1113AAD C.A.B.A., Argentina.

[b]Consejo Nacional de Investigaciones Científicas y Técnicas, Instituto de Química y Fisicoquímica Biológicas, Buenos Aires, Argentina

[c]Center for Theoretical Biological Physics, Rice University, Houston, TX 77005.

[d]Universidad de Buenos Aires, Facultad de Ciencias Exactas y Naturales, Intendente Güiraldes 2160 - Ciudad Universitaria, 1428EGA C.A.B.A., Argentina.

[e]Universidad de Buenos Aires. Consejo Nacional de Investigaciones Científicas y Técnicas. Instituto de Química Biológica de la Facultad de Ciencias Exactas y Naturales (IQUIBICEN). Facultad de Ciencias Exactas y Naturales.

*To whom correspondence should be addressed: lgf@ffyb.uba.ar and ernest.roman@gmail.com

Running title: Cracking modulates the ATPase activity of AfCopA-CD.

**Keywords.**

$P_{IB}$-type ATPases, Catalytic Domain, Local unfolding, ATPase activity, Local frustration

# Abstract

Membrane transporters are essential for cell homeostasis. Among them P-type ATPases, which couple ATP hydrolysis to solute transport, play a key role. Despite extensive research, the fine mechanisms by which this coupling occurs are not completely understood. In this work, we analyzed the effect of substrate, temperature, and urea on the steady state ATPase activity, tryptophan fluorescence and far-UV ellipticity of the catalytic domain of a thermophilic Cu(I) transport ATPase. Through local frustration analysis in combination with AlphaFold2 prediction, we identified a novel conformation, enabling molecular dynamics simulations of an open/close transition. Our results revealed a “cracking” mechanism as a key step in the catalytic cycle. Furthermore, we developed a model that fully describes all the experimental observations. These findings reinforce the idea that local unfolding is involved in enzyme catalysis and suggest a key role in the regulation of enzyme activity.

# Introduction

An important part of the proteins encoded in genomes are membrane proteins [1,2]. Since these membrane proteins are difficult to obtain in a purified form in the laboratory, the knowledge gained about them is much less compared to their soluble counterparts [3]. Among these proteins the transporters are essential for cell homeostasis and communication with the environment by binding a ligand in one side of the membrane and translocating it to the other side [4,5]. In the case of active transport, this is done by transducing the highly exergonic ATP hydrolysis into work involved in conformational changes that are coupled to ligand transport [6–8]. One of the most studied active transport families is the P-ATPases which bind ATP and couple its hydrolysis to solute transport across membranes with a phosphorylated intermediate that gives the name to these families [9] . Although there are many representative structures from different subfamilies, organisms and transported solutes, most of the structural and mechanistic information comes from the $Ca^{2+}$ ATPase [10–13], the $Na^{+}/K^{+}$ ATPase [14–16], and -in a lesser extent- the $Cu^{+}$ ATPase [9,17–21]. Their structures share a transmembrane domain, through which the substrate is transported, and cytoplasmic domains that consist of a catalytic modulator (A or "actuator") and an ATP catalytic domain (CD) comprised by the N ("nucleotide binding") and P ("phosphorylation") subdomains [22,23] (Figure S1). Hitherto, the fine structural mechanism by which the energy transduction occurs remains elusive.

*Archaeoglobus fulgidus* CopA (*Af*CopA) is a thermophilic Cu(I)-transport ATPase that belongs to the subfamily of $P_{1B}$ ATPases, which are involved in heavy metal ion homeostasis. This 804 amino acid long protein can be heterologously expressed in *E. coli*, purified and reconstituted in a functional form, retaining its thermophilic [24] and thermostable [3,25,26] features. The catalytic domain (AfCopA-CD), is located on the cytoplasmic side and contains 265 amino acids. This domain was successfully expressed and crystallized (25), and the resulting structure shows good congruence with that of the full-length protein. Up to our knowledge, the only laboratories that reported structural information and ATPase activity for CD of P-ATPases are the ones working with Cu(I) transport ATPases: CopA from *Archaeoglobus fulgidus* (*AfCopA*-CD) [27] and *Thermotoga maritima (Tm*CopA-CD*)*

[28], and CopB from *Archaeoglobus fulgidus* (*Af*CopB-CD) [29]. The *Af*CopA-CD has been crystallized in the absence and presence of ATP [30]. Surprisingly, both structures are in their closed state, even in the absence of the ligand [29]. However, TmCopA-CD has been obtained in the bound and closed states, whereas AfCopB-CD has only been obtained in the unbound and open state. As the protein needs both subdomains to be in contact with the ligand to hydrolyze ATP and be phosphorylated, it is relevant to understand how the conformational change involved in open-close transition is regulated and involved in protein activity. The understanding of how large conformational transitions linked to triphosphate-nucleotide hydrolysis are coupled with the generation of work has been the goal of experimental and theoretical approaches [31–33]. In many cases regions are subjected to high stress and, to transition from one conformation to the other, the strain must be released with a local unfolding reaction usually known as ‘cracking’ [32–35]. One way to experimentally test this mechanism has been the use of chaotropes to lower the activation barrier for the local unfolding step [35,36].

In this work, we characterized the effect of substrate concentration and temperature on *Af*CopA-CD steady-state ATPase activity, as well as the impact of temperature and urea on its ATPase activity, intrinsic fluorescence, and far-UV ellipticity. We studied the role of local frustration in the open-close transition and combined this tool with AlphaFold2 to predict the previously unreported open structure. With the aid of molecular dynamics simulations we studied the role of strain and “cracking”. Our results point to local unfolding involved in enzyme catalysis and suggest a role of cracking in temperature optimum activity regulation.

# Results and Discussion

**Temperature differentially affects the ATP apparent affinity and the catalytic constant of the enzyme-catalyzed ATP hydrolysis.**

As was mentioned, *Af*CopA-CD is one of the soluble domains of the Copper transport P-ATPase from the hyperthermophilic organism *Archaeoglobus fulgidus*, *Af*CopA. To assess whether this domain, when isolated, conserves its native features and to gain insights into its catalytic mechanism, we evaluated the effect of temperature and substrate concentration on the steady state ATP hydrolysis (Figure 1).

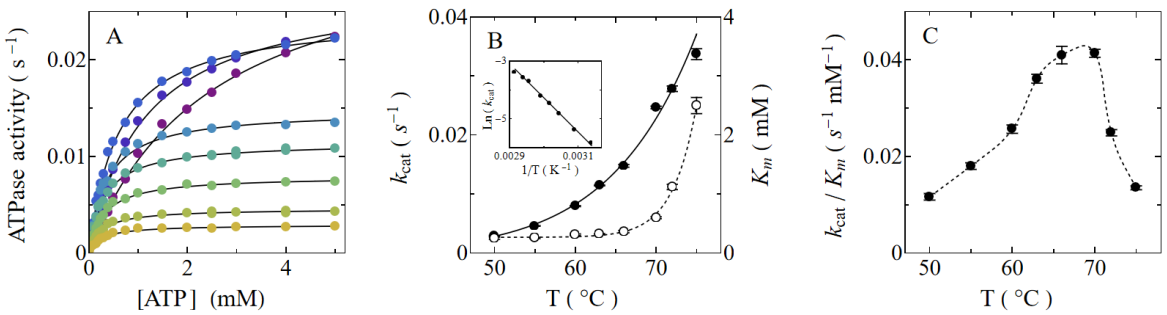


Figure 1. *AfCopA-CD* ATPase activity at different temperatures. ***A***. ATP concentration dependence of ATPase activity at different temperatures 75 (●), 72 (●), 70 (●), 66 (●), 63 (●), 60 (●), 55 (●), and 50°C (●), respectively. Continuous lines are the graphical representations of equation 1 fitted to the experimental data of each curve. ***B.*** *Af*CopA-CD catalytic constant ($k_{cat}$ , ●) and Michaelis-Menten constant ($K_m$ , ○ ) as a function of temperature. Continuous line is the graphical representation of the Arrhenius equation ($k_{cat} = A \cdot e^{-Ea/RT}$ ) with the best fitting values of A ($1.14 \cdot 10^{13} \pm 9.10^{-16}$ $s^{-1}$) and Ea (23.07 ± 0.02 kcal/mol). Dashed line constitutes a guide to the eye. Inset shows the corresponding Arrhenius plot. **C**. Catalytic efficiency ($k_{cat}/K_m$) as a function of temperature. Dashed line constitutes a guide to the eye.

It can be observed that ATPase activity follows a hyperbolic function of ATP concentration (Figure 1A):

$$molar\ ATPase\ activity = \frac{k_{cat}[ATP]}{K_m + [ATP]} \quad (1)$$

The catalytic constant ($k_{cat}$) increases with temperature (Figure 1B) and can be described by the Arrhenius equation. In the examined temperature range it does not evidence any curvature that would suggest a change in the catalytic mechanism. The activation energy ($E_a$) obtained was 23.07 ± 0.02 kcal $mol^{-1}$ and is approximately two-times the $E_a$ of the entire *Af*CopA ATPase (14 ± 1 kcal $mol^{-1}$) [24]. This finding is

reflected in the $k_{cat}$ observed for the isolated domain which is lower than the one corresponding to the full-length *Af*CopA[37]. Additionally, the Michaelis-Menten constant ($K_m$) also increases with temperature (Figure 1B), indicating a decrease of the apparent affinity for ATP. The different trends of the effect of temperature on $K_m$ and $k_{cat}$ yield a catalytic efficiency ($k_{cat}/K_m$) (Figure 1C) with a maximum around 70°C which is close to the observed optimal growth temperature of *Archaeoglobus fulgidus* [38]. Notably, although the domain is in its isolated form, not only it remains catalytically active at the optimal working temperature of the full-length *Af*CopA as was previously mentioned somewhere else [27,28], but also the apparent affinity for ATP (0.25 ± 0.04 mM) is conserved.

## Tryptophan fluorescence and far-UV molar ellipticity evidence a complex energy landscape for the native ensemble of conformations

To evaluate the functionally related conformational ensemble of *Af*CopA-CD we performed a temperature ramp experiment followed by tryptophan intrinsic fluorescence and far-UV ellipticity, both transitions being reversible. It is worth mentioning that the *Af*CopA-CD has a single tryptophan residue located at position 576 (full-length *Af*CopA numbering) which is in the interface between N and P subdomains (Figure 2A). This suggests that intrinsic fluorescence might be perfectly suited to monitor relative movements between both subdomains.

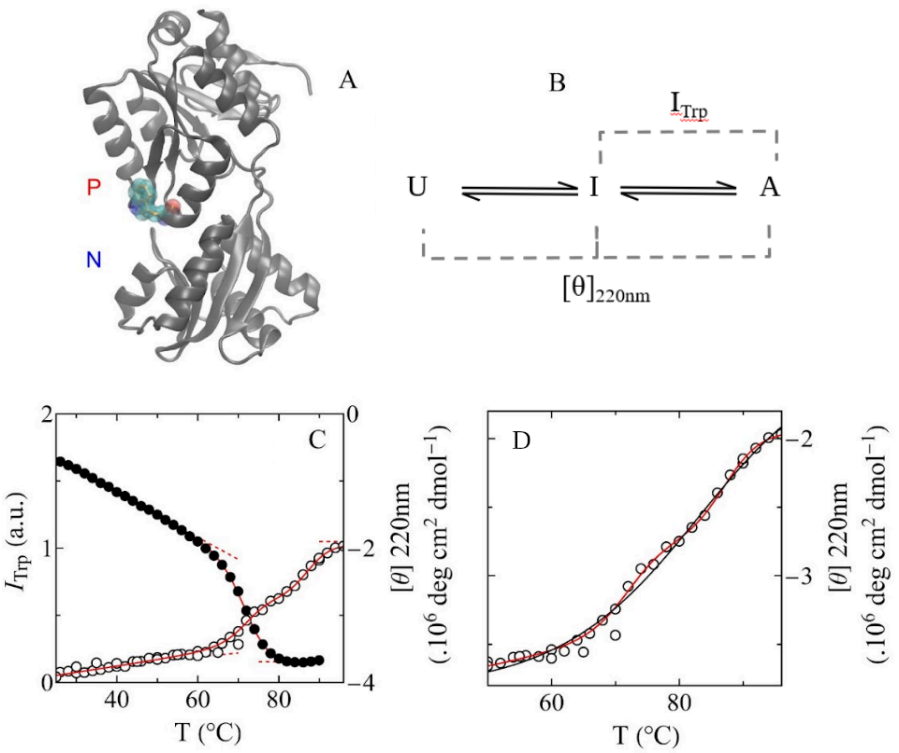


Figure 2. Spectroscopic analysis of *Af*CopA-CD at different temperatures. **A.** Structure representation of the PDB ID 3A1C chain A highlighting the tryptophan 576 of the *Af*CopA-CD (full-length *Af*CopA numbering) surrounded by its Van der Waals volume. Image was built using VMD software [39]. **B.** Three-states equilibrium model. The active state A is in equilibrium with an intermediate state termed I and an unfolded state U. Dashed lines represent which transition is monitored with fluorescence (ITrp ) and ellipticity ([θ]220nm). **C.** Intrinsic tryptophan fluorescence (●) and far-UV molar ellipticity at 220 nm (○) as a function of temperature. Continuous red lines are the graphical representations of the three-states model equation (equation S2) fitted to both curves simultaneously (best fit parameter values are shown in table S1). Dashed lines represent the pre- and post-transition slopes. **D.** Zoom of panel C showing the best fits of two- (black lines) and three-states (red lines) model equations (equations S1 and S2, respectively) to the far-UV molar ellipticity at 220 nm as a function of temperature.

Total fluorescence intensity decreases as a function of temperature, while the center of the spectral mass shifts to a higher wavelength (from around 352 nm to 355 nm), indicating an increase of the tryptophan solvent exposure. Although the fluorescence intensity changes can be described by a two-state model (Equation S1), far-UV molar ellipticity dependence is better described by a three-states equilibrium model. Thus, both fluorescence and far-UV ellipticity were well described using the three states model shown in Figure 2B (Equation S2, see AICc values in Table S6).

The transition occurring at the lowest mid-denaturing temperature ($T_{m\ A\text{-}I}$), both monitored by fluorescence and far-UV molar ellipticity, has a value of approximately 70°C (Figure 2C-D, Table S1) while the second transition has a $T_{m\ I\text{-}U}$ around 85°C. Notably, the transition from A to I occurs with only partial loss of secondary structure and coincides with the temperature range where *Af*CopA-CD is active (Figure 1C). It

is noteworthy that the loss in secondary structure is about half of the expected for total unfolding. Thus, this suggests that partially folded species may be relevant to the catalytic cycle. In contrast, the second transition (from I to U) is associated with a significant loss of secondary structure, indicative of protein denaturation.

## Small additions of urea enhances enzyme-catalyzed ATP hydrolysis suggesting a local unfolding mechanism related to catalysis

To monitor the link between ATP catalyzed hydrolysis and conformational rearrangements, we evaluated the effect of urea in *Af*CopA-CD activity at different temperatures (Figure 3). Surprisingly, at all temperatures tested, ATPase activity increases with urea concentration while decreasing at higher concentrations.The urea concentration where the maximum ATPase activity is observed increases as temperature decreases.

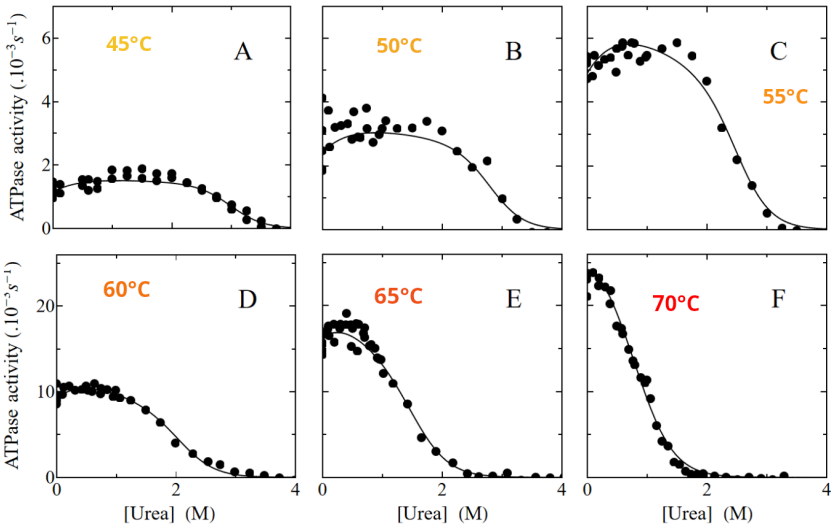


Figure 3. *Af*CopA-CD ATPase activity at different temperatures and urea concentrations. **A-F**. ATPase activity was determined at different temperatures (45, 50, 55, 60, 65, 70°C, respectively for each panel) in the presence of 3 mM ATP, 30 mM $MgCl_2$ and 5 μM enzymes. For ATPase activity assays in the presence of urea, the protein was incubated for at least 40 min prior to the reaction. Continuous lines are the graphical representation of the equation derived from the model in Figure 9F (Equation S9) fitted to both spectroscopic and molar ATPase activity data at all temperatures, ATP and urea concentrations assayed. Best fit parameter values are shown in Table S4.

In the presence or absence of urea, ATPase activity increases with ATP concentration following a hyperbolic function (Figure S3). The $K_m$ of the reaction increases with urea occurring without a decrease of the ATPase activity. This reveals that there is an increase in the apparent $k_{cat}$ at low urea concentrations. The

behaviour of the apparent $k_{cat}$ as a function of temperature in the absence and low urea concentrations is shown in Figure 4.

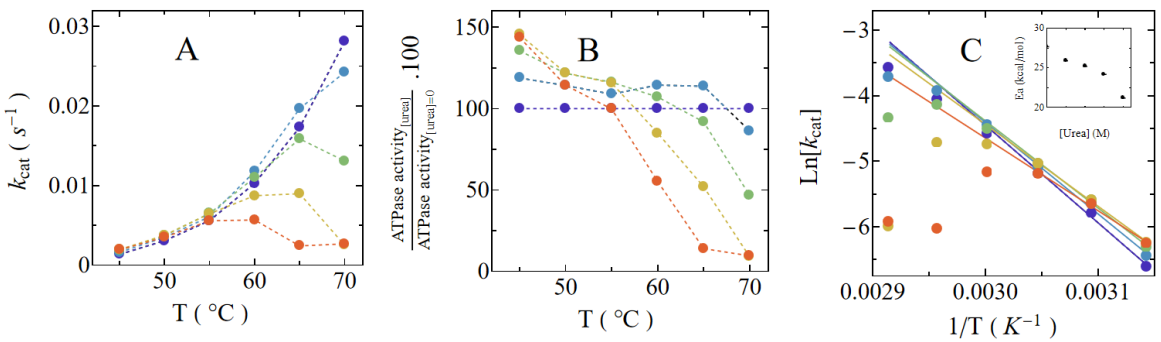


Figure 4. *Af*CopA-CD ATPase $k_{cat}$ at different temperatures and urea concentrations. **A.** *Af*CopA-CD apparent ATPase $k_{cat}$ determined at 0 (●), 0.5 (●), 1 (●), 1.5 (●) and 2 M urea (●) as a function of temperature. **B.** Percentual ATPase activity increases at the different urea concentrations relative to the value obtained in absence of urea (ATPase activity $_{[Urea]}$ /ATPase activity $_{[Urea]=0}$) as a function of temperature. **C.** Arrhenius plot of the $k_{cat}$ at the different urea concentrations. Lines are the graphical representations of the Arrhenius equation fitted to the $k_{cat}$ as a function of the temperature in the range 45-55°C at the assayed urea concentrations. Inset shows the corresponding best fitting values of $E_a$ as a function of urea. The coloring scheme is the same for the entire figure. In all cases, dashed lines constitute a guide for the eye.

It can be observed that the temperature at which the catalytic constant is the highest decreases with the addition of urea (Figure 4A). When expressed as a percent of the activity in the absence of urea, there are increases of up to 50% of the activity in the range between 40 and 50°C (Figure 4B). Interestingly, although occurring at all temperatures, the increase in the apparent $k_{cat}$ is more pronounced at the lowest temperatures assayed. At each urea concentration, the increase of $k_{cat}$ with temperature can be described by the Arrhenius equation (Figure 4C). It is noteworthy that the addition of small amounts of urea lowers the activation energy of the reaction. This result suggests that the rate limiting step of ATP catalysis is sensitive to small amounts of chaotropic agents.

The conditions at which activation by urea occurs were also evaluated using tryptophan intrinsic fluorescence and far-UV ellipticity at different urea concentrations and temperatures (Figure 5).

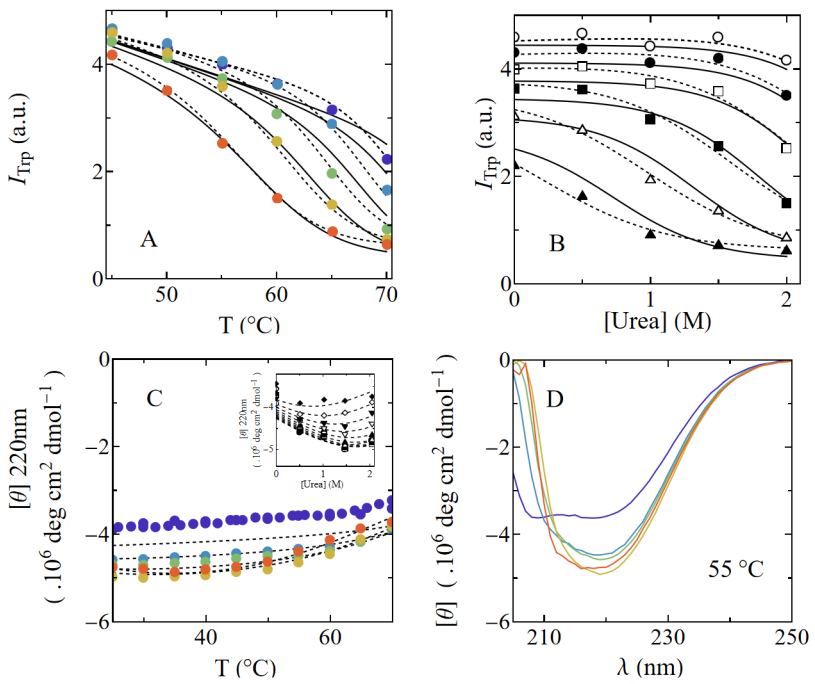


Figure 5. Spectroscopic analysis of *Af*CopA-CD at the temperatures and urea concentrations evaluated. **A.** Intrinsic tryptophan fluorescence as a function of temperature in the presence of 0 (●), 0.5 (●), 1 (●), 1.5 (●) and 2 M urea (●). **B**. Intrinsic fluorescence intensity as a function of urea concentration at 45 (○), 50 (●), 55 (□), 60 (■), 65 (△) and 70 (▲) °C. In both panels A and B, dashed lines are the graphical representations of a two-states model (equation S1) fitted to all curves simultaneously, with the best fit parameter values shown in table S2. Continuous lines are the graphical representation of the equations derived from the model in Figure 9F (Equation S8) simulated with the best fitting values shown in Table S5. **C.** Far-UV molar ellipticity at 220 nm as a function of temperature in the presence of the different urea concentrations. Inset shows the behavior as a function of urea concentration. Dashed lines constitute a guide for the eye. **D.** Far-UV ellipticity spectra at 55°C and the different urea concentrations. The coloring scheme is the same for the entire figure. When the measurements were performed in the presence of urea, the protein was incubated for at least 40 min prior to the reaction.

It is noteworthy that the conformational change evidenced by Trp fluorescence occurs at lower temperatures when small urea amounts were added. Similarly, fluorescence monitored transition shifts to lower urea concentrations as temperature increases (Figure 5B). These changes are in line with the position of the maximum activity, suggesting a coupling between the observed increase in ATPase activity and this change. When molar ellipticity at 220 nm was evaluated as a function of temperature (Figure 5C), there is no evidence of protein unfolding. Nevertheless, it is noteworthy that when urea concentrations as low as 0.5 M were added, there is a large change in the far-UV ellipticity spectra as seen in Figure 5D.

The increase in catalytic activity in the presence of low denaturant concentrations has already been described for a small set of proteins including adenylate kinase, dihydrofolate reductase, prostaglandin D synthase, biliverdin-IXα reductase and

papain [40–49]. In general this phenomena is interpreted as the modulation of the transition barrier connecting functional conformations in a way that small additions of chaotropes lower its energy making the exchange between conformations more favorable. Although theoretical studies of the mechanism are supported by experimental evidence, they are largely limited to adenylate kinase [42–45] and, to a lesser extent, dihydrofolate reductase [40,41]. Up to our knowledge, the *Af*CopA-CD is a new experimental model to study the effect of local unfolding in catalytic mechanisms.

## Tryptophan fluorescence captures conformational transitions that are linked to enzyme catalysis

As previously mentioned, the single tryptophan residue of the *Af*CopA-CD is located at the interface between the N and P subdomains (Figure 2A) with a calculated surface exposed to the solvent of 50 % [50]. This result is in agreement with the measured center of spectral mass of approximately 351 nm (at 25°C). When Trp fluorescence is evaluated as a function of urea concentration for a given temperature (i.e. 55°C, Figure 6A), total intensity abruptly changes, with a mid-denaturant concentration ($C_m$) of 2.15 ± 0.03 M at 55°C.

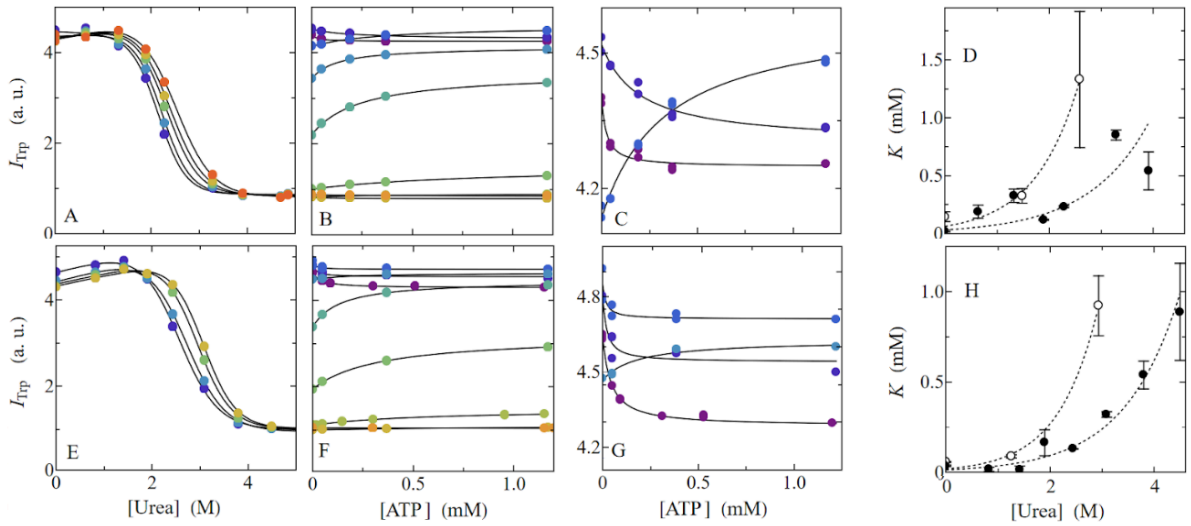


Figure 6. Effects of temperature and urea on the *Af*CopA-CD Trp fluorescence intensity. **A** and **E.**Total intensity ($I_{Trp}$) at different urea concentrations at 55°C (Panel A) and 0 (●), 0.05 (●), 0.2 (●), 0.4 (●) and 1.2 mM ATP (●) or at 45°C (Panel E) and 0 (●), 0.05 (●), 0.3 (●) and 1.2 mM ATP (●). Continuous lines are the graphical representation of equation S1 fitted to each curve. **B** and **F**. Total intensity ($I_{Trp}$) at different ATP concentrations at 55°C (Panel B) and 0 (●), 0.6 (●), 1.3 (●), 1.9 (●), 2.3 (●), 3.3 (●), 4.0 (●) and 4.8 M urea (●) or at 45°C and 0 (●), 0.83 (●), 1.42 (●), 1.9 (●), 2.44 (●), 3.09 (●), 3.8 (●), 4.5 (●) and 5.3 M urea (●). Continuous lines are the graphical representation of equation S5 fitted to each curve. **C** and **G**. A zoom of panels B and F shows the corresponding behavior at low urea concentrations. **D** and **H**. Dissociation constant $K_{ATP}$ values(●) obtained from the

best fit of equation S5 to Trp fluorescence intensity dependence on ATP concentration at 55 and 45°C respectively. Panels also show ATPase activity $K_m$ (o) obtained from the best fit of equation 2 to ATPase activity dependence on ATP concentration as a function of urea concentration at the same temperatures (Figure S3). Dashed lines are the graphical representation of exponential functions fitted to each curve.

The center of spectral mass also changes abruptly, from approximately 351 nm to 356 nm (Figure S4), showing an increase in solvent exposure. Addition of ATP shifts the $C_m$ towards higher urea concentration values which evidence ATP binding to *Af*CopA-CD (Figure 6A and S4). Interestingly, ATP has a dual effect on fluorescence intensity. While at low concentrations it quenches the emission, at higher concentrations it increases it, suggesting the existence of an equilibrium of species with different quantum yields (Fig 6B and 6C). This overall behaviour is maintained at all the evaluated temperatures (Fig 6E-G). These results suggest that fluorescence is monitoring at least two partially independent phenomena. This is not surprising since tryptophan fluorescence would be monitoring the relative movement between subdomains, while ATP binding takes place in the N-subdomain as has been previously characterized for the CopA human homologue [51]. Considering binding of a single ATP molecule per protein, at each urea concentration, apparent affinity for ATP ($K_{ATP}$) can be obtained using equation S1. As can be seen in Figures 6D and 6H, $K_{ATP}$ increases with urea concentration.

## Local frustration is linked to open-close transition

As discussed by *Jayakanthan et al*., ATP binding to most P-ATPases catalytic domain induces a rotation of both N and P subdomains yielding a more compact conformation and resulting in a decrease of the binding site solvent exposition. Structural studies of *Af*CopA-CD have shown only closed conformations [27,28]. However, it is reasonable to presume the existence of an open state which has been reported to be relevant to the catalytic mechanism [29]. Energy landscape theory provides a thorough framework for analyzing protein folding and conformational transitions [52]. These transitions occur in a funneled landscape where roughness appears as patches of highly frustrated contacts which are usually involved in conformational transitions and functional dynamics [53]. Frustration patches in the closed structure of the *Af*CopA-CD, in the presence of an ATP analogue (PDB ID 3A1C), are mainly located at the interface between N and P subdomains (Figures 7A and 7C). To assess whether these patches are involved in conformational transitions,

we followed the protocol implemented by Guan et al [31]. Briefly, after identifying most frustrated positions in the structure with the bound ligand we masked them using gaps in the alignment that feeds AlphaFold2. The top scored prediction revealed a conformation where the *Af*CopA-CD binding site is exposed to the solvent (Figures 7B). Interestingly, when no masking was applied, the best ranked structure superimposes perfectly to the previously solved crystal structure.

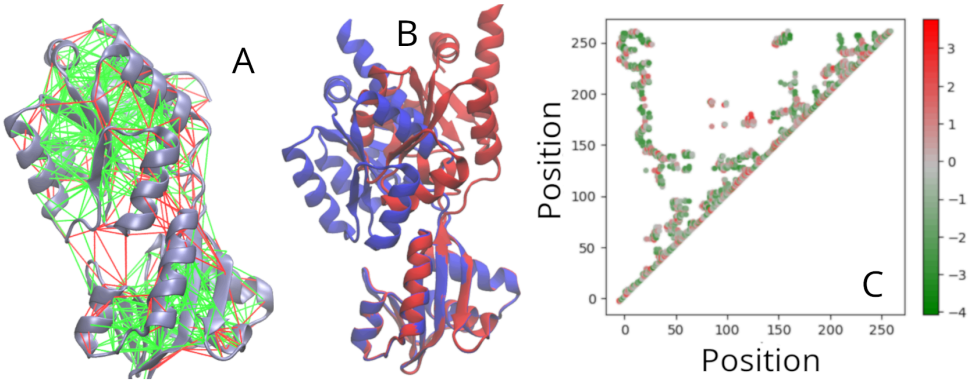


Figure 7. Effect of frustration in the conformational transition between the reported closed and the predicted open conformation. **A**. Mutationally frustrated contacts were calculated using the Frustratometer server [54] and are displayed on the *Af*CopA-CD closed state. Red and green lines correspond to the highly and minimally frustrated contacts, respectively. **B**. AF2 prediction of the open (red) and experimentally reported closed (blue) conformations. **C**. Contact map of the closed state colored by mutational frustration index. Each point corresponds to an interatomic interaction and the color scale describes the local frustration index. Position numbering is according to the *Af*CopA-CD sequence.

To characterize the transition between both conformations, we performed structure-based α-carbon simulations using an in-house implementation of the forcefield described in [55]. To explore the dynamics of the open-to-close movement we performed umbrella sampling guided simulations using the difference in the RMSD between the closed (PDB ID 3A1C) and the AF2/Local frustration-predicted open structure (Figure 7B red) as the reaction coordinate ($RMSD_{difference}$). We analyzed the results considering the contacts that are formed exclusively in the closed conformation ($Q_{ligand}$ ) and $RMSD_d$ coordinates. Varying the energy weight of the $Q_{ligand}$ ($\varepsilon_{Qligand}$) populates the open ($\varepsilon_{Qligand}$ = 0) or the closed state ($\varepsilon_{Qligand}$ = 1) (Figure S5). When $\varepsilon_{Qligand}$ = 0.8 the resulting free energy landscape shows three main basins being the open (low $Q_{ligand}$ and low $RMSD_d$), a partially closed (intermediate $Q_{ligand}$ and high $RMSD_d$) and a closed (high $Q_{ligand}$ and high $RMSD_d$) states (Figure 8A). Free energy profiles with different $\varepsilon_{Qligand}$ values are shown in Figure S5. Interestingly, the partially closed conformation appears with a slight disruption of ligand-mediated contacts (Figure 8B and equation S13).

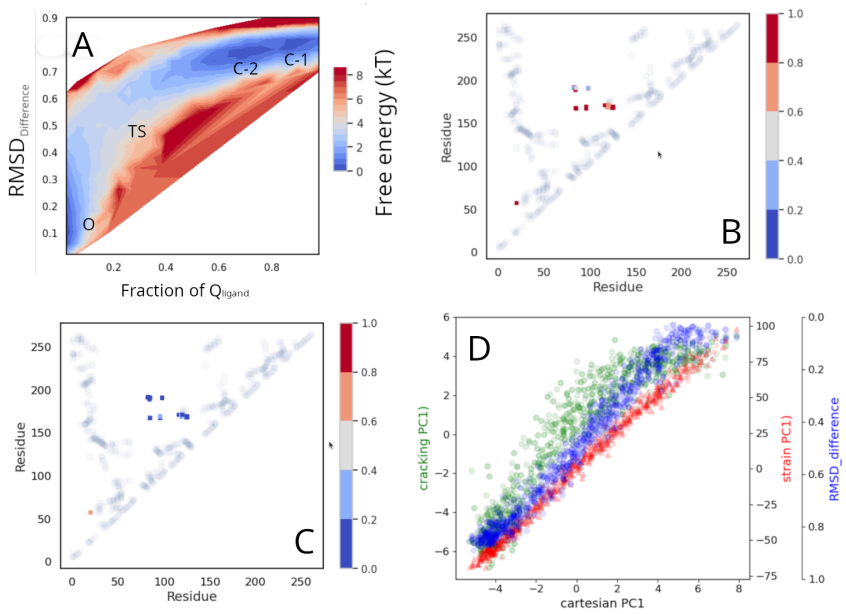


Figure 8. Energy Landscape of the open - close transition of the *Af*CopA-CD. **A**. Free Energy profile using the fraction of $Q_{ligand}$ and $RMSD_{difference}$ as reaction coordinates at $\varepsilon_{Qligand}$ = 0.8. The color represents the free energy in kT units. Labels indicate open (O), transition (TS), partially closed (C-2) and closed conformations (C-1). **B**. Contact α-values for the C-2 conformation (equation S13). **C**. Contact α-values for the TS (equation S13). Position numbering in panels B and C is according to the *Af*CopA-CD sequence. **D**. Correlation of the projections of the PC1 of Cracking (green), strain (red) to the trajectory, and $RMSD_{difference}$ (blue) with the projection of the cartesian first principal component to the trajectory.

This implies that destabilizing those contacts favors a partially closed state prior to the opening transition. This may be mimicking the addition of urea which at below denaturing concentrations can destabilize the already formed contacts. The transition state, on the contrary, has most of the $Q_{ligand}$ disrupted as can be seen in Figure 8C. The addition of urea at small concentrations then would favour the partially closed conformation making the opening transition more favorable. A picture of the main ensemble of conformations can be seen in Figure S6.

To analyze the conformational change we calculated the strain and cracking principal components as described in Methods [31]. The largest-amplitude principal component on interatomic distances (strain) and formation or rupture of native contacts (cracking) show that the involved contacts are those with highest frustration index (Figures S7 and 7C). Figure 8D shows a perfect correlation between the PC1 based on the cartesian coordinates, the strain PC1 (red) and the $RMSD_{difference}$ (blue dots) indicating that the component is describing the same transition monitored in the simulation. The increase in the strain PC1 also correlates with the opening of the *Af*CopA-CD (low values of $RMSD_{difference}$) indicating a stressing $Q_{ligand}$ interface. It can

also be seen that the cracking PC1 (green dots) stops increasing after a certain value which reveals the breakage of $Q_{ligands}$. All these results point to a cracking mechanism linked to the functional movements. The finding of a partially closed (partially open) state as a consequence of a decrease in the $\varepsilon_{Qligand}$ may be explaining the urea induced increase in ATPase activity.

## ATPase activation is a consequence of the accumulation of a reaction intermediate

To gain insights into the coupling between ATP hydrolysis and conformational changes we analyzed both the spectroscopic and activity results with a model that comprises two states, I and A, where only A is able to bind ATP and catalyze its hydrolysis (Figure 9E, Equations S6 and S7). Although this model is able to explain the change of intrinsic fluorescence with urea and ATP, the activation exerted by the addition of small urea amounts is not captured (Figure 9, gray dotted line). Moreover, if we follow the approach described by Rogne et al. [43] making $k_{AATP}$ dependent on urea concentration, we can explain the ATPase activity increase but we fail to describe the intrinsic fluorescence change and the apparent affinity for ATP (Figure 9, red dotted line). Alternatively, we developed a model (Figure 9F) that incorporates one additional ATP bound species, IATP, in equilibrium with AATP, with only the latter catalytically active. The model was solved under rapid-equilibrium assumption for all steps ($K_2=k_{-2}/k_2$, Equations S8 and S9). Interestingly, although this model explains our results, it does not fully explain both ATP concentration dependences of enzyme activation and intrinsic fluorescence. However, when the ATP binding step is considered out of the rapid equilibrium condition (Equation S10) both spectroscopic and ATPase activities are fully explained (Figure 9 solid line for 55°C and Figure S9 for 45°C). Notably, the fact that this step is out of the rapid equilibrium condition yields a difference in $K_m$ and $K_{ATP}$ dependence on urea concentration (Figure S8), which is responsible for better describing our experimental observations as evaluated using AICc (Table S7). The best fit parameter values are shown in Table S4.

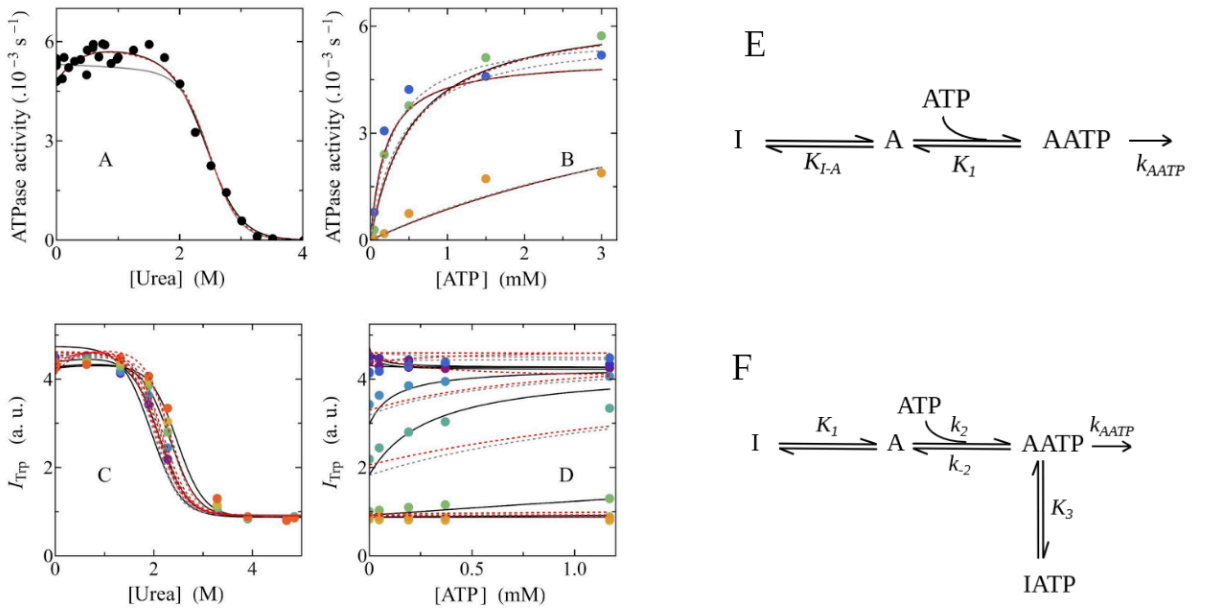


Figure 9. Description of the effect of ATP and urea on ATPase activity and Trp fluorescence at 55°C. **A-D**. Gray and red lines are the graphical representations of the global fitting of equations derived from model in panels E (equations S6 and S7) and F (equations S8 and S9) to the experimental results previously shown in Figures 3A, 6E-F and S2, both under the rapid equilibrium assumption. Black lines are the graphical representations of the equations derived from Panel F without assuming rapid equilibrium conditions (equations S8 and S10), fitted to the experimental results. **E**. Reaction model of *Af*CopA-CD catalytic activity with only one ATP binding step. A is in equilibrium with a reaction intermediate state termed I and is able to bind ATP to give AATP, which is the catalytically active species. **F**. Reaction model of AfCopA-CD catalytic activity with two ATP bound species but only one catalytically active. The state A is in equilibrium with a reaction intermediate termed I. When the model is solved under the assumption of rapid equilibrium k-2/k2 is replaced by the equilibrium constant K2. State A is able to bind ATP and populate two species, AATP and IATP, where only AATP is active.

The molar fractions of each species in different conditions were obtained from the corresponding model derived equations and the best fit parameter values from Table S4 (Figure S11). The activating effect of low urea concentrations is exerted by an increase of the concentration of species AATP with respect to IATP. The equilibrium among these species and their slightly different quantum yield, account for the effect observed on Trp fluorescence. At higher urea concentrations, dissociation of ATP is favoured, with the uppermost displacement of the equilibrium between A and I, giving place to the decrease in ATPase activity and the total intensity fluorescence. Interestingly, the *m-values*, which are the dependence of each constant with the urea concentration, are compatible with partial unfolding reactions (A to I in Figure 9F). A small *m-value* corresponding to ATP binding (A to AATP) suggests a small change of accessible surface upon binding. In contrast, the *m-value* when moving from IATP to AATP suggests that the productive AATP state is less compact than IATP. Figure 5D

shows that upon urea addition there is a large and reversible change in secondary structure which is compatible with stabilization of beta sheets and destabilization of helical motifs. This change coincides with the urea concentrations where activation occurs. Furthermore, we evaluated whether this model was also able to describe the temperature dependent observations. Temperature dependence of the step governed by $K_1$ required inclusion of the heat capacity change to fully describe our results. This is reasonable given the large change in accessible surface area associated to that step (Table S7).

Moreover, when considering the effect of temperature, the model not only describes ATPase activity dependence on urea concentration (continuous lines in Figures 3) at all assayed temperatures, but also predicts Trp fluorescence dependence on both factors (continuous lines in figure 5A and 5B). The fact that the urea activating effect is lower at the highest temperatures can now be explained by decrease in the accumulation of AATP as the temperature increases (Figure S12). The best fit value of $E_a$ of the catalytic step (31 ± 1 kcal $mol^{-1}$) is of the order of that obtained from the dependence of $k_{cat}$ with temperature (Figure 1C - 23.07 ± 0.02 kcal $mol^{-1}$) which reinforces the robustness of our modelistic description of the reaction.

# Concluding remarks

Our results highlight the intricate regulation of *Af*CopA-CD ATPase activity by temperature and small amounts of urea. The temperature-dependent changes in ATP apparent affinity ($K_m$) and catalytic turnover ($k_{cat}$) resulted in a biphasic catalytic efficiency profile, with an optimal temperature of approximately 70°C. The linearity of the Arrhenius plot across all conditions indicates a consistent reaction mechanism, despite variations in temperature and urea concentration. Notably, the unexpected enhancement of ATPase activity by small amounts of urea, contrasting with its typical denaturing effects, suggests a local unfolding mechanism that facilitates catalysis. Supporting this idea, local frustration analysis reveals that the interface between the nucleotide binding and phosphorylation subdomains is enriched in frustrated contacts whose masking in the AlphaFold2 alignment aided in the prediction of an alternative structure for the *Af*CopA-CD. This predicted open structure allowed us to simulate the open-to-close transition which involves the rupture of those interfacial frustrated contacts. This result gives support to the crucial role of local frustration in enzyme catalysis and structural transitions. Taking this into account, the activation by small amounts of urea may come, at least in part, from the disruption of these contacts with high contact order and local frustration index. As the transition state has almost none of the $Q_{ligand}$ the disruption by small amounts of urea may favour the open close transition by diminishing the barrier height. Thus, the experimentally observed effect on affinity and catalytic parameters seems to be the consequence of the local frustration present in the *Af*CopA-CD energy landscape.

Intrinsic fluorescence and spectroscopic analyses evidence the strong link between conformational transitions and enzyme catalysis in *Af*CopA-CD. ATP titrations showed significant induced changes in intrinsic fluorescence, consistent with the location of the enzyme single tryptophan residue at the interface between both subdomains, likely reflecting ATP binding events. However, in the presence of urea, ATP titrations not only showed a decrease in binding affinity but also the presence of distinct ATP-bound species in equilibrium. Complementary fluorescence experiments at different temperatures displayed a single conformational transition whereas ellipticity revealed at least two, with the first one aligning with the fluorescence-derived $T_m$ and the second occurring at higher temperatures.

Surprisingly, ellipticity at concentrations below 0.5 M revealed a critical conformational change, underlining the complexity of *Af*CopA-CD's conformational dynamics. Altogether these experiments provided complementary insights into the native conformational ensemble energy landscape and emphasize the intricate relationship between structural transitions and catalytic function.

The integration of our observations in a single mechanistic-equilibrium model offers a unified explanation for the observed phenomena suggesting that small perturbations, such as urea or temperature changes, disrupt the subdomain interface, lowering the activation barrier for conformational transitions and thereby modulating enzymatic activity. The identification of a previously unrecognized reaction intermediate provides new insights into the activation mechanism and explains the increase in ATPase activity induced by urea as a result of the accumulation of this intermediate, highlighting its critical role in facilitating catalysis. In this sense, the finding of a partially closed conformation in the simulations may be related to one of the ATP bound conformations described in the model. As this conformation is partially closed, addition of urea could be loosening the tight formed interface favoring in some way the increase in activity. These results underscore the delicate balance of structural and energetic factors driving enzyme function and regulation.

Finally, this work provided a comprehensive understanding of the interplay between temperature, urea, and conformational dynamics in modulating the activity of AfCopA-CD. We give a plausible explanation of all our experimental observations with the aid of molecular dynamics simulations and local frustration analysis combined with a mathematical mechanistic analysis. The findings underscored the significance of intermediate states, local frustration, local unfolding and conformational flexibility in enzymatic regulation, offering valuable insights into the fundamental principles governing protein function. The open question is whether this mechanism occurs in the context of the full-length protein serving a role in the native functional dynamics. Further experimental and computational efforts are needed to determine whether this mechanism is a common feature in all P-ATPases.

# Materials and methods

## Materials

Yeast extract and soybean tryptone were purchased from Britania (Buenos Aires, Argentina). Ampicillin was purchased from BioBasic (Toronto, Canada). Lactose, Tris and Imidazole were purchased from Anedra (Buenos Aires, Argentina). Buffer MES, NaCl, ATP and $MgCl_2$ were from Merck (Darmstadt, Germany). Urea was purchased from MPbiomedichals (California, USA).

## Cloning of AfCopA-CD

*Af*CopA-CD (from K407 to K671 using AfCopA numbering [24]) was cloned into the pPR-IBA1vector (IBA). The resulting construction (274 residues) contained a small linker followed by a 6xHis tag at the C-terminus of the protein [27]. Cloning was confirmed by DNA sequencing of the plasmid amplicon.

## Strains, media and growth conditions

*Escherichia coli Bl21 Star (DE3) pLysS* strain was used for protein expression. Bacteria were grown at 37 °C in Luria Bertani broth (LB: 1% NaCl, 1% tryptone, and 0.5% yeast extract), supplemented with 100 µg/mL Ampicillin. Briefly, 25 ml LB media were inoculated with stock *Bl21 Star (DE3) pLysS Af*CopA-CD bacteria overnight at 37 °C with constant shaking. The culture was then diluted up to 0.01 absorbance units in 1l fresh LB media and growth at 37 °C with constant shaking up 0.6-0.8 absorbance units. At this point protein expression was induced by the addition of 10% Lactose and incubation continued for 3.5 hours. Cells were harvested by centrifugation and frozen at -80 °C until protein purification.

## *Af*CopA-CD purification

Cells were resuspended in 50 mM Tris pH 7.5 at 4°C and 500 mM NaCl (buffer A) plus 10 mM Imidazole and 1 mM phenylmethylsulfonyl fluoride. Lysis was performed by sonication using 8 pulses of 30 seconds separated by 1 minute of sample rest at 4 °C. Afterwards the suspension was sedimented for 15 minutes at 8.000*g* and 4°C. Supernatant was heated for 15 minutes at 55°C and centrifuged again for 30 minutes

at 10000*g* for precipitation of thermolabile proteins as described in [28]. The resulting supernatant was loaded in a Ni-NTA column and washed with 50 column volumes of Buffer A plus 20 mM Imidazole. Elution was done with buffer A plus 300 mM imidazole and followed by intrinsic tryptophan fluorescence. Fractions containing the protein were pooled and Imidazole was removed by overnight dialysis or passing the sample through a chromatographic column containing Sephadex G-25 equilibrated with storage solution (50 mM Tris pH 7,5 and 150 mM NaCl) and stored at -80 °C. Protein purity was evaluated by SDS-PAGE and its concentration was estimated by light absorbance at 280 nm ($\varepsilon_{280nm}$ 5500 $M^{-1}cm^{-1}$) [56].

## Fluorescence measurements

Steady-state fluorescence measurements were performed in a Jasco FP-6500 spectrofluorometer equipped with a Peltier thermostatic cell holder. To this end, a 0.3 cm path length cell sealed with a Teflon cap was used. The excitation wavelength was 295 nm and emission data was collected in the range of 305–430 nm. The spectral slit-width was set to 3 nm for both monochromators.

## Circular dichroism spectroscopy

Ellipticity of protein samples was evaluated using a Applied Photophysics Chirascan V100 spectropolarimeter equipped with a Peltier thermostatic cell holder. Far-UV circular dichroism spectra were recorded in the range between 205 and 250 nm, protein concentration was 10 μM, and a cell of 1 mm path-length was used. Data was acquired at a scan speed of 4 nm $s^{-1}$. Blank scans were subtracted from the spectra and molar ellipticity was expressed in units of deg $cm^2$ $dmol^{-1}$.

## Protein unfolding experiments

After incubation for at least 40 min at room temperature, *Af*CopA-CD isothermal unfolding experiments were carried out in 0–2 M urea in a buffer solution (25 mM MES pH 5.5 at 70°C, 100 mM NaCl). The process was followed by far-UV ellipticity and tryptophan fluorescence. Thermal unfolding experiments were performed by varying the temperature from 25 to 70°C or 96°C, at a rate of 1°C $min^{-1}$. Equations used for the analysis are described in *Supplementary Information*.

## ATPase activity measurements

ATPase activity of *Af*CopA-CD was determined by measuring the amount of inorganic phosphate (*Pi*) released from ATP at different reaction times at different temperatures otherwise stated on each figure. *Pi* concentration was determined spectrophotometrically according to a modified Malachite Green method [57,58]. Reaction media contained protein concentrations of 4-6 uM, 25 mM MES pH 5.5 at 70°C, 100 mM NaCl, 30 mM $MgCl_2$ and 3 mM ATP unless otherwise indicated. Initial rate was calculated from the time course of *Pi* release, measured in at least 5 independent reactions and expressed with their respective standard error. Background ATP hydrolysis was subtracted to all measurements. Molar ATPase activity was calculated dividing the initial rate by enzyme concentration.

## Model selection

To evaluate the goodness of the model fit we used the Second-Order Akaike Information Criterion (AICc) which is defined as:

$$AICc = N \times ln\left(\frac{SS}{N}\right) + \frac{2\,N\,K}{(N-K-1)},$$

with N = number of data, K = number of parameters plus 1, and SS = sum of weighted square residual errors [59]. The best equation was considered to be the one which gave the lower value of AICc.

## Computational methods

### *AlphaFold2 prediction*

AlphaFold2 (AF2) was used to predict the open conformation of the *Af*CopA-CD. We followed the protocol described in Guan et al. [31] by first calculating highly frustrated positions in the *Af*CopA-CD (PDB 3A1C A) structure and masking those positions in the AF2 alignment. Local Frustration analysis was performed using Frustratometer 2 server [54].

### *Structure-based model simulations*

We performed dual-basin Cα-Structure-based model simulations (Cα-SBM) using an in-house OpenMM implementation with a force field parameterization described in [60]. We used native bonds, angles and dihedrals corresponding to the open structure predicted using AF2 in combination with local frustration calculations [31]. As we evaluated the free energy landscape of the open-to-closed transition, we modeled the presence of the ligand as the contacts in the closed conformation (PDB ID 3A1C) that are 50% further apart in the open conformation ($Q_{ligand}$ - Figure S2). Thus, native contacts were defined within 2 different basins: the contacts of the open state, with a corresponding energy weight of 1 ($\varepsilon_{nc}$=1); and the $Q_{ligand}$, with energy weight variable ($\varepsilon_{Qligand}$). The closing reaction was simulated by increasing the $\varepsilon_{Qligand}$ favouring the closed conformation as in [60,61]. We biased the simulation from the open to the closed state by employing Umbrella Sampling technique using the difference in the root-mean squared deviation ($RMSD_{dif}$) between the reference closed and open states [31]. The reaction coordinate was calculated using:

$$RMSD_{difference}(rmsd_o, rmsd_c) = \frac{(rmsd_{vs\ open} - rmsd_{vs\ closed} + rmsd_{open\ vs\ closed})}{2\, rmsd_{open\ vs.\ closed}}$$

where $rmsd_{vs\ open}$ and $rmsd_{vs\ closed}$ are the calculated root-mean squared deviation of the current structure with respect to the open and closed states, respectively; $rmsd_{open\ vs\ closed}$ is a constant value representing the root-mean squared deviation between the reference open and closed states. Free energy profiles were obtained by performing several constant temperature simulations and combining them using the Weighted Histogram Analysis Method (WHAM) [62]. All results in this work are at T = 0.9-0.8 in reduced units (kT = 1). Principal components analysis (PCA) was performed using sklearn python library [63] taking two different approaches. On one side, in strain PCA, the covariance matrix was built on the basis of interatomic distance variations among the simulation ($d_{ij}$) between the Cα atoms of two residues, while on the other side, in cracking PCA the covariance matrix was built using a binary definition of contacts and described the fluctuation of the contacts formation; when $d_{ij}$ > 1.2 * native distance the value is 0 while it is 1 otherwise.

**Acknowledgements**. This work was funded by *CONICET* (PIP 2022). We thank Dr. José M. Arguello's (Worcester Polytechnique Institute, Worcester, MA, USA) for sharing the *Af*CopA-CD plasmid. We also thank Dr. Diego U. Ferreiro (Universidad de Buenos Aires) for carefully reading and discussing this manuscript. Additionally, we acknowledge Facundo Balerdi Roman for critical reading. Finally, we manifest our deep concerns about the sudden discontinuation of scientific funding which impedes the development of new projects and terminates the current ones.

**Conflict of Interest**: Authors declare that they have no conflict of interest.

# References


1. Wallin E, von Heijne G. Genome-wide analysis of integral membrane proteins from eubacterial, archaean, and eukaryotic organisms. Protein Sci. 1998;7: 1029–1038. doi:10.1002/pro.5560070420

2. Fagerberg L, Jonasson K, von Heijne G, Uhlén M, Berglund L. Prediction of the human membrane proteome. PROTEOMICS. 2010;10: 1141–1149. doi:10.1002/pmic.200900258

3. Recoulat Angelini AA, Roman EA, González Flecha FL. The Structural Stability of Membrane Proteins Revisited: Combined Thermodynamic and Spectral Phasor Analysis of SDS-induced Denaturation of a Thermophilic Cu(I)-transport ATPase. Journal of Molecular Biology. 2024;436: 168689. doi:10.1016/j.jmb.2024.168689

4. Gulezian E, Crivello C, Bednenko J, Zafra C, · Zhang Y, Colussi P, et al. Membrane protein production and formulation for drug discovery. Trends in Pharmacological Sciences. 2021;42: 657–674. doi:10.1016/j.tips.2021.05.006

5. Yin H, Flynn AD. Drugging Membrane Protein Interactions. Annu Rev Biomed Eng. 2016;18: 51–76. doi:10.1146/annurev-bioeng-092115-025322

6. Ramm B, Goychuk A, Khmelinskaia A, Blumhardt P, Eto H, Ganzinger KA, et al. A diffusiophoretic mechanism for ATP-driven transport without motor proteins. Nature Physics. 2021;17: 850–858. doi:10.1038/s41567-021-01213-3

7. Nath S. Coupling and biological free-energy transduction processes as a bridge between physics and life: Molecular-level instantiation of Ervin Bauer's pioneering concepts in biological thermodynamics. Biosystems. 2024;236: 105134. doi:10.1016/j.biosystems.2024.105134

8. Gao F, Guo J, Si Q, Wang L, Zhang F, Yang F. Modification of ATP hydrolysis by Strong Coupling with O−H Stretching Vibration. ChemPhotoChem. 2023 [cited 26 Dec 2024]. doi: https://doi.org/10.1002/cptc.202200330

9. Dyla M, Kjærgaard M, Poulsen H, Nissen P. Structure and Mechanism of P-Type ATPase Ion Pumps. Annu Rev Biochem. 2020;89: 583–603. doi:10.1146/annurev-biochem-010611-112801

10. Kabashima Y, Ogawa H, Nakajima R, Toyoshima C. What ATP binding does to the Ca2+ pump and how nonproductive phosphoryl transfer is prevented in the absence of Ca2+. Proceedings of the National Academy of Sciences. 2020;117: 18448–18458. doi:10.1073/pnas.2006027117

11. Boczek T, Sobolczyk M, Mackiewicz J, Lisek M, Ferenc B, Guo F, et al. Crosstalk among Calcium ATPases: PMCA, SERCA and SPCA in Mental Diseases. Int J Mol Sci. 2021;22. doi:10.3390/ijms22062785

12. Xu J, Wang Y. Generating Multistate Conformations of P-type ATPases with a Conditional Diffusion Model. J Chem Inf Model. 2024;64: 9227–9239. doi:10.1021/acs.jcim.4c01519

13. Geurts MMG, Clausen JD, Arnou B, Montigny C, Lenoir G, Corey RA, et al. The SERCA residue Glu340 mediates interdomain communication that guides Ca2+ transport. Proc Natl Acad Sci U S A. 2020 [cited 26 Dec 2024]. doi:10.1073/pnas.2014896117

14. Kumari J, Rathore MS. Na+/K+-ATPase a Primary Membrane Transporter: An Overview and Recent Advances with Special Reference to Algae. The Journal of Membrane Biology. 2020;253: 191–204. doi:10.1007/s00232-020-00119-0

15. Lopina OD, Bukach OV, Sidorenko SV, Klimanova EA. Na+,K+-ATPase As a Polyfunctional Protein. Biochemistry (Moscow), Supplement Series A: Membrane and Cell Biology. 2022;16: 207–216. doi:10.1134/S1990747822040055

16. Contreras RG, Torres-Carrillo A, Flores-Maldonado C, Shoshani L, Ponce A. Na+/K+-ATPase: More than an Electrogenic Pump. International Journal of Molecular Sciences. 2024;25: 6122.

doi:10.3390/ijms25116122

17. Dyla M, Basse Hansen S, Nissen P, Kjaergaard M. Structural dynamics of P-type ATPase ion pumps. Biochem Soc Trans. 2019;47: 1247–1257. doi:10.1042/BST20190124

18. Dmitriev OY, Patry J. Structure and mechanism of the human copper transporting ATPases: Fitting the pieces into a moving puzzle. Biochimica et Biophysica Acta (BBA) - Biomembranes. 2024;1866: 184306. doi:10.1016/j.bbamem.2024.184306

19. Guo Z, Orädd F, Bågenholm V, Grønberg C, Ma JF, Ott P, et al. Diverse roles of the metal binding domains and transport mechanism of copper transporting P-type ATPases. Nature Communications. 2024;15: 1–16. doi:10.1038/s41467-024-47001-4

20. Fodor I, Yañez-Guerra LA, Kiss B, Büki G, Pirger Z. Copper-transporting ATPases throughout the animal evolution – From clinics to basal neuron-less animals. Gene. 2023;885: 147720. doi:10.1016/j.gene.2023.147720

21. Placenti MA, Roman EA, González Flecha FL, González-Lebrero RM. Functional characterization of Legionella pneumophila Cu transport ATPase. The activation by Cu and ATP. Biochim Biophys Acta Biomembr. 2022;1864: 183822. doi:10.1016/j.bbamem.2021.183822

22. Palmgren M. P-type ATPases: Many more enigmas left to solve. Journal of Biological Chemistry. 2023;299: 105352. doi:10.1016/j.jbc.2023.105352

23. Stock C, Heger T, Basse Hansen S, Thirup Larsen S, Habeck M, Dieudonné T, et al. Fast-forward on P-type ATPases: recent advances on structure and function. Biochem Soc Trans. 2023;51: 1347–1360. doi:10.1042/BST20221543

24. Mandal AK, Cheung WD, Argüello JM. Characterization of a thermophilic P-type Ag+/Cu+-ATPase from the extremophile Archaeoglobus fulgidus. J Biol Chem. 2002;277: 7201–7208. doi:10.1074/jbc.M109964200

25. Cattoni DI, González Flecha FL, Argüello JM. Thermal stability of CopA, a polytopic membrane protein from the hyperthermophile Archaeoglobus fulgidus. Arch Biochem Biophys. 2008;471: 198–206. doi:10.1016/j.abb.2007.12.013

26. Roman EA, Argüello JM, González Flecha FL. Reversible unfolding of a thermophilic membrane protein in phospholipid/detergent mixed micelles. J Mol Biol. 2010;397: 550–559. doi:10.1016/j.jmb.2010.01.045

27. Sazinsky MH, Mandal AK, Argüello JM, Rosenzweig AC. Structure of the ATP binding domain from the Archaeoglobus fulgidus Cu+-ATPase. J Biol Chem. 2006;281: 11161–11166. doi:10.1074/jbc.M510708200

28. Tsuda T, Toyoshima C. Nucleotide recognition by CopA, a Cu+-transporting P-type ATPase. EMBO J. 2009;28: 1782–1791. doi:10.1038/emboj.2009.143

29. Jayakanthan S, Roberts SA, Weichsel A, Argüello JM, McEvoy MM. Conformations of the apo-, substrate-bound and phosphate-bound ATP-binding domain of the Cu(II) ATPase CopB illustrate coupling of domain movement to the catalytic cycle. Biosci Rep. 2012;32: 443–453. doi:10.1042/BSR20120048

30. Sazinsky MH, Mandal AK, Arguello JM, Rosenzweig AC. CopA ATP Binding Domain. Worldwide Protein Data Bank; 2006. doi:10.2210/pdb2b8e/pdb

31. Guan X, Tang Q-Y, Ren W, Chen M, Wang W, Wolynes PG, et al. Predicting protein conformational motions using energetic frustration analysis and AlphaFold2. Proc Natl Acad Sci U S A. 2024;121: e2410662121. doi:10.1073/pnas.2410662121

32. Orädd F, Ravishankar H, Goodman J, Rogne P, Backman L, Duelli A, et al. Tracking the ATP-binding response in adenylate kinase in real time. Sci Adv. 2021;7: eabi5514. doi:10.1126/sciadv.abi5514

33. Alavi Z, Casanova-Morales N, Quiroga-Roger D, Wilson CAM. Towards the understanding of molecular motors and its relationship with local unfolding. Q Rev Biophys. 2024;57: e7. doi:10.1017/S0033583524000052

34. Fan YX, Ju M, Zhou JM, Tsou CL. Activation of chicken liver dihydrofolate reductase by urea and guanidine hydrochloride is accompanied by conformational change at the active site. Biochem J. 1996;315 ( Pt 1): 97–102. doi:10.1042/bj3150097

35. Miyashita O, Onuchic JN, Wolynes PG. Nonlinear elasticity, proteinquakes, and the energy landscapes of functional transitions in proteins. Proc Natl Acad Sci U S A. 2003;100: 12570–12575. doi:10.1073/pnas.2135471100

36. Onuchic JN, Kobayashi C, Miyashita O, Jennings P, Baldridge KK. Exploring biomolecular machines: energy landscape control of biological reactions. Philosophical Transactions of the Royal Society B: Biological Sciences. 2006 [cited 26 Dec 2024]. doi:10.1098/rstb.2006.1876

37. Bredeston LM, González Flecha FL. The promiscuous phosphomonoestearase activity of Archaeoglobus fulgidus CopA, a thermophilic Cu transport ATPase. Biochimica et Biophysica Acta (BBA) - Biomembranes. 2016;1858: 1471–1478. doi:10.1016/j.bbamem.2016.04.006

38. Klenk H-P, Clayton RA, Tomb J-F, White O, Nelson KE, Ketchum KA, et al. The complete genome sequence of the hyperthermophilic, sulphate-reducing archaeon Archaeoglobus fulgidus. Nature. 1998;390: 364–370. doi:10.1038/37052

39. Humphrey W, Dalke A, Schulten K. VMD: Visual molecular dynamics. Journal of Molecular Graphics. 1996;14: 33–38. doi:10.1016/0263-7855(96)00018-5

40. Fan YX, Ju M, Zhou JM, Tsou CL. Activation of chicken liver dihydrofolate reductase in concentrated urea solutions. Biochim Biophys Acta. 1995;1252: 151–157. doi:10.1016/0167-4838(95)00125-e

41. Fan Y, Zhu L, Zhou J, Zou C. Sequential conformation change and activation of chicken liver dihydrofolate reductase in low concentration of guanidine hydrochloride. Science in China Series C: Life Sciences. 1997;40: 202–209. doi:10.1007/BF02882049

42. Zhang HJ, Sheng XR, Pan XM, Zhou JM. Activation of adenylate kinase by denaturants is due to the increasing conformational flexibility at its active sites. Biochemical and biophysical research communications. 1997;238. doi:10.1006/bbrc.1997.7301

43. Rogne P, Wolf-Watz M. Urea-Dependent Adenylate Kinase Activation following Redistribution of Structural States. Biophys J. 2016;111: 1385–1395. doi:10.1016/j.bpj.2016.08.028

44. Rastogi H, Singh A, Chowdhury PK. Towards the energy landscape of adenylate kinase in crowded milieu: Activity, conformation, structure and dynamics in sequence. Archives of Biochemistry and Biophysics. 2023;743: 109658. doi:10.1016/j.abb.2023.109658

45. Scheerer D, Levy D, Casier R, Riven I, Mazal H, Haran G. Enzyme activation by urea reveals the interplay between conformational dynamics and substrate binding: a single-molecule FRET study. bioRxiv. 2024. p. 2024.09.01.610662. doi:10.1101/2024.09.01.610662

46. Inui T, Ohkubo T, Urade Y, Hayaishi O. Enhancement of lipocalin-type prostaglandin D synthase enzyme activity by guanidine hydrochloride. Biochem Biophys Res Commun. 1999;266: 641–646. doi:10.1006/bbrc.1999.1881

47. Franklin E, Mantle T, Dunne A. Activation of human biliverdin-IXα reductase by urea: generation of kinetically distinct forms during the unfolding pathway. Biochimica et biophysica acta. 2013;1834. doi:10.1016/j.bbapap.2013.09.009

48. Inui T, Ohkubo T, Emi M, Irikura D, Hayaishi O, Urade Y. Characterization of the unfolding process of lipocalin-type prostaglandin D synthase. The Journal of biological chemistry. 2003;278. doi:10.1074/jbc.M209934200

49. Hill RL, Schwartz HC, Smith EL. The effect of urea and guanidine hydrochloride on activity and optical rotation of crystalline papain. J Biol Chem. 1959;234: 572–576. Available: https://www.ncbi.nlm.nih.gov/pubmed/13641262

50. Mitternacht S. FreeSASA: An open source C library for solvent accessible surface area calculations. F1000Research. 2016;5: 189. doi:10.12688/f1000research.7931.1

51. Rodriguez-Granillo A, Sedlak E, Wittung-Stafshede P. Stability and ATP binding of the nucleotide-binding domain of the Wilson disease protein: effect of the common H1069Q mutation. J Mol Biol. 2008;383: 1097–1111. doi:10.1016/j.jmb.2008.07.065

52. Wolynes PG, Eaton WA, Fersht AR. Chemical physics of protein folding. Proceedings of the National Academy of Sciences. 2012;109: 17770–17771. doi:10.1073/pnas.1215733109

53. Ferreiro DU, Komives EA, Wolynes PG. Frustration in biomolecules. Q Rev Biophys. 2014;47: 285–363. doi:10.1017/S0033583514000092

54. Parra RG, Schafer NP, Radusky LG, Tsai M-Y, Guzovsky AB, Wolynes PG, et al. Protein Frustratometer 2: a tool to localize energetic frustration in protein molecules, now with electrostatics. Nucleic Acids Res. 2016;44: W356–60. doi:10.1093/nar/gkw304

55. Clementi C, Nymeyer H, Onuchic JN. Topological and energetic factors: what determines the structural details of the transition state ensemble and “en-route” intermediates for protein folding? an investigation for small globular proteins. Journal of Molecular Biology. 2000;298: 937–953. doi:10.1006/jmbi.2000.3693

56. Pace CN, Vajdos F, Fee L, Grimsley G, Gray T. How to measure and predict the molar absorption coefficient of a protein. Protein Sci. 1995;4: 2411–2423. doi:10.1002/pro.5560041120

57. Martínez Gache SA, . Recoulat Angelini AA, Sabeckis ML, González Flecha FL. Improving the stability of the malachite green method for the determination of phosphate using Pluronic F68. Anal Biochem. 2020;597: 113681. doi:10.1016/j.ab.2020.113681

58. Recoulat Angelini AA, Martínez Gache SA, Sabeckis ML, Melian NA, González Flecha FL. On the role of citrate in 12-molybdophosphoric-acid methods for quantification of phosphate in the presence of ATP. New J Chem. 2022;46: 12401–12409. doi:10.1039/D2NJ00943A

59. Burnham KP, Anderson DR. Model Selection and Multimodel Inference: A Practical Information-Theoretic Approach. Springer, New York; 2002.

60. Whitford PC, Miyashita O, Levy Y, Onuchic JN. Conformational transitions of adenylate kinase: switching by cracking. J Mol Biol. 2007;366: 1661–1671. doi:10.1016/j.jmb.2006.11.085

61. Jayanthi LP, Mascarenhas NM, Gosavi S. Structure dictates the mechanism of ligand recognition in the histidine and maltose binding proteins. Curr Res Struct Biol. 2020;2: 180–190. doi:10.1016/j.crstbi.2020.08.001

62. de Oliveira AB Jr, Contessoto VG, Hassan A, Byju S, Wang A, Wang Y, et al. SMOG 2 and OpenSMOG: Extending the limits of structure-based models. Protein Sci. 2022;31: 158–172. doi:10.1002/pro.4209

63. Garreta R, Moncecchi G, Hauck T, Hackeling G. scikit-learn : Machine Learning Simplified: Implement scikit-learn into every step of the data science pipeline. Packt Publishing Ltd; 2017. Available: https://play.google.com/store/books/details?id=sEFPDwAAQBAJ